METHODOLOGY APPLIED TO STUDY WATER MIST AS AN INFRARED SIGNATURE SUPPRESSOR IN MARINE GAS TURBINES

Reference NO. IJME 815, DOI: 10.5750/ijme.v165iA1.815

J M Pernas Urrutia, University of La Coruña, Spain; **R Villa Caro,** University of La Coruña, Spain; **R Perez-Fernandez,** Polytechnic University of Madrid, Spain and **F Hernández,** University of New South Wales, Australia

KEY DATES: Submission date: 03.12.21 / Final acceptance date: 30.03.23

SUMMARY

This paper proposes a methodology for the reduction of marine gas turbine exhaust gas temperatures via water mist injection into exhaust gas ducts with the aim of reducing a ship's infrared (IR) signature. Due to the difficulty of conducting live experimental tests on warships, Computational Fluid Dynamic (CFD) techniques can be employed to predict phase interaction behaviour (water mist and exhaust gases) within gas turbine exhausts. CFD techniques attempt to find numerical solutions to the equations that govern phase interaction phenomena through the setting and resolution of mathematical models. This alternative allows the replacement of conventional eductor-difuser based supression systems, confirming the viability of further development of the proposed methodology for its impact on the IR signature of a warship.

NOMENCLATURE

AIAA	American Institute of Aeronautics and Astronautics
ASMD	AntiShip Missile Defence
CFD	Computational Fluids Dynamics
CODOG	COmbined Diesel Or Gas turbine
DE	Diesel Engines
DPM	Discrete Phase Model
DSU	Data Storage Unit
DVD	Digital Versatile Disc
ECM	Electronic CounterMeasures
FAT	Factory Acceptance Test
FLIR	Forward Looking InfraRed
GT	Gas Turbine
HMI	Human Machine Interface
IR	InfraRed
LWIR	Long Wavelength InfraRed
MVD	Median Volumetric Diameter
MWIR	Medium Wavelength InfraRed
PCS	Propulsion Control System
PL	Power Level
RANS	Reynolds Averaged Navier-Stokes
SAT	Sea Acceptance Test

1. INTRODUCTION

It is believed that the Canadian Navy in the late 1930s was the first to attempt to reduce the signature of its ships via diffused lighting camouflage in the visible range. This honour is also often awarded to the German submarine U-480, employing a rubber coating and a layer of airbags to remain undetected by allied sonar.

Since then, signature reduction has become a tactical military discipline employing primarily passive countermeasures encompassing a wide range of techniques used in air, naval and ground warships, and even human combatants themselves. The objective is to employ camouflage to boost stealth, for example, in different ranges of the electromagnetic spectrum, so as not to be detected by radar, sonar, and IR devices.

Infrared radiation, closely associated with heat emission and transmission, is used in multiple defence applications, particularly in detection cameras and anti-ship weapon guidance systems. To counteract the threat of these weapons, a warship's IR signature must be minimised through the reduction of heat emission to the environment.

In the case of a warship, the atmosphere provides an attenuating effect on the IR energy emitted, absorbing it in its totality across the entire spectrum with the exception of two distinct bands, namely MWIR "*Medium Wavelength Infra-Red*" with wavelengths between 3 and 5 μm and LWIR "*Long Wavelength InfraRed*" with wavelengths between 8 and 12 μm. These two bands are characterized by high transmittance due to low atmospheric attenuation (Greig, et al. 2009).

Exhaust gases are predominantly a source of IR radiation in the MWIR band, used primarily by IR guidance weapons. Exhaust gases also contribute to IR emission in the LWIR, albeit in a lower capacity, used primarily by night vision systems to detect, classify and track targets via thermographic cameras such as FLIR "*Forward Looking InfraRed*" (Greig, et al. 2009).

A modern warship's repertoire of countermeasures for the reduction of its IR signature, includes eductors/diffusers for the cooling of both the final stages of exhaust ducts, as well as the exhaust gases of internal combustion engines

themselves (mainly gas turbines and diesel engines) (Thompson, et al. 2000).

In order to maximize cooling of internal combustion engine exhaust gases, saltwater sprayers are being added to traditional eductor/diffuser cooling systems to create hybrid prototypes (Hiscoke, 2002).

Adoption of these hybrid systems represents the current trend in the development of IR signature suppression in naval warships:

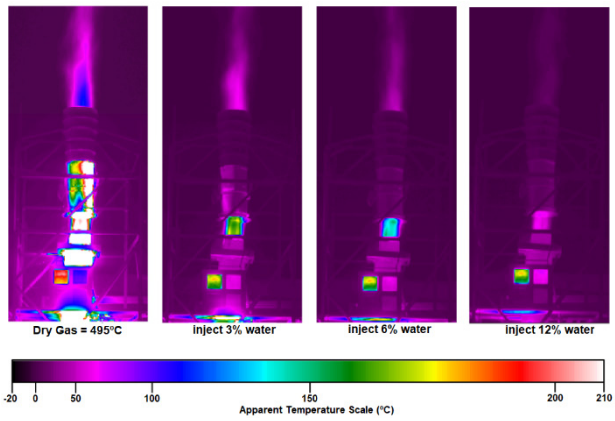

Figure 1. Infrared Images of Prototype Hybrid System. Source: Hiscoke, 2002

This paper summarises the methodology used, based on employment of CFD techniques, to demonstrate the feasibility of combining two technologies – gas turbine (GT) exhaust systems and water mist – with the aim of reducing the IR signature of a a surface warship.

To accomplish this, real GT running data is required as an input to the calculations and simulations involved in the proposed methodology.

Similarly, the study of interaction between continuous (exhaust gas flow) and discrete (water mist) phases requires the definition of *"initial"* and *"boundary conditions*" for both phases.

Of equal importance is selection of domain discretization criteria in the study of the continuous phase (meshing). The study of the discrete phase requires the separation of two types of initial conditions: *"fixed"* and *"variable"*, thus enabling sequential variation of the latter in order to observe the effect these changes have on the model's final calculated results.

The proposed methodology also requires the development and establishment of operational requirements for inclusion in surface warship ASMD (*"AntiShip Missile Defence"*) doctrine.

Concretely, requirements for integration into the ECM (*"Electronic CounterMeasures"*) subsystem must be determined, as an additional technique in the suite of countermeasures known as *"deception techniques"*.

These techniques are employed in high speed operations, and subsequent system dimensioning must include requirements for compatibility with the high speed demands of ASMD operations.

Elevated GT lever settings are predicted, in order to respond to the high speeds demanded by this type of operations.

2. THEORETICAL BACKGROUND

2.1 CODOG CONFIGURATION

A single CODOG "*COmbined Diesel Or Gas turbine*" shaft line configuration is chosen for collection of GT exhaust gas data for input into subsequent flow simulation of the proposed model. The CODOG configuration selection is composed of the following commercial engines, a GT and a diesel engine (DE), in widespread use in surface warship propulsion:

– One (1) GT General Electric LM2500 (GE, 1999).
– One (1) DE Caterpillar C280-16 (CAT, 2010).

This CODOG propulsion configuration enables a 6000 tonne destroyer to achive a cruise speed (transit) of approximately 18 knots in DE mode, with both shaft lines at 80% of the DE's max continuous power (9 bMW), and a sprint speed of 28 knots in GT mode, with both shaft lines at 100% of the GT's maximum continuous power (35 bMW).

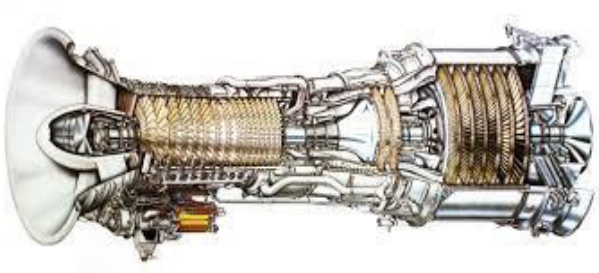

Figure 2. Longitudinal Section of GT LM2500. Source: GE, 1999

2.2 GT OPERATION DATA COLLECTION PROCESS

The GE LM2500 GT's running data is collected from the following sources:

- FAT results taken at manufacturer's installation
- CODOG configuration surface warship SAT results.
- CODOG configuration surface warship HMI running data.
- Bibliographic references (GE, 1999).

A surface warship's PCS (*"Propulsion Control System"*), which monitors and remotely controls propulsion related equipment and services, stores running data DSU (*"Data Storage Unit"*). This data can later be accessed to visualise equipment/system behaviour, compile data, analyse failures and conduct security copies to DVD (*"Digital Versatile Disc"*) (Wärtsilä, 2017).

Figure 3 below summarises air inlet (T1) and outlet (T7) temperatures compiled from GT running data:

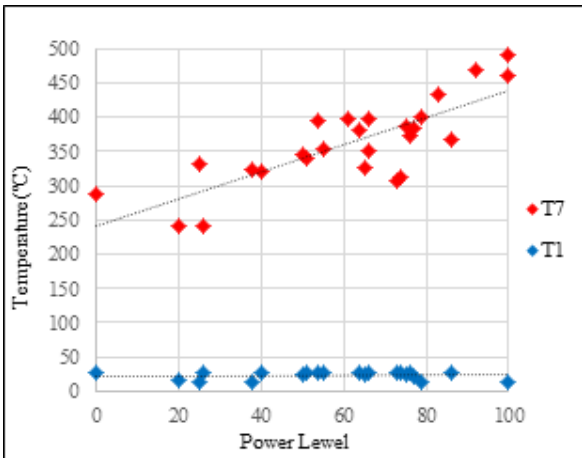

Figure 3: Intake (T1) and Exhaust (T7) temperatures of GT LM2500. Source: Own Elaboration

2.3 FLOW MODELING IN GT EXHAUST DUCT

Computational fluid dynamics or CFD is used to attempt to predict fluid behaviour, heat and mass transfer phenomena, and chemical reactions through numerical solutions of the governing equations of the distinct processes in play (Bakker, 2002).

Numerical solution of a given fluid flow problem requires the following general steps to be followed (Ballesteros, et al. 2003):

- Establishment of simulation objectives or "*goals*".
- Creation of model geometry and subsequent meshing, commonly referred to as *"domain discretization"*.
- Configuration of the physical models and solver (*"initial conditions"* and *"boundary conditions"*).
- Computational solution of the problem, and solution monitoring (convergence study).
- Study of post-CFD results.
- Review of physical and numerical parameters of the model, as required.

The problem solution and monitoring phase, which includes discretization and linearization of the governing equations, is further broken down into the following steps (Bhaskaran, 2018):

- Establishment of boundary conditions and governing equations in differential form.
- Transformation of governing equations from differential to integral forms.
- Derivation of a system of algebraic equations related to the values of flow variables at the centre of the domain's cells (discretization)
- Transformation of the system of cell-centre referenced equations to a system of linear algebraic equations (linearization)
- Solution of the system of linear algebraic equations via iterative methods, with continuous updating of the set points.
- Finalization of the iterative process occurs when variable values barely vary from the previous iteration values (convergence)

It is to be noted, that the processes of domain discretization (meshing) and linearization of the algebraic equations contain implicit errors, governed by selection of mesh size (discretization) and selection of the residual convergence values (linearization). These errors must be taken into account when seeking an accurate numerical solution of the problem (Bhaskaran, 2018).

2.4 CONTINOUS PHASE GEOMETRY AND MESHING

In order to simplify the geometry of the model, a 12 metre long, 2m diameter, cylindrical exhaust duct is selected. The duct is assumed to be aligned with the GT, is located immediately after, and its diameter corresponds to the power turbine's exhaust gas diameter:

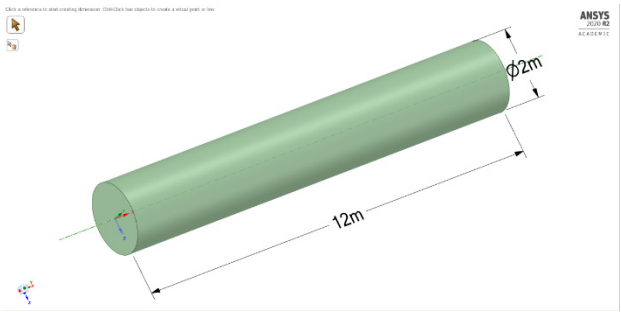

Figure 4. 3D Geometry of Exhaust Duct. Source: Courtesy ANSYS Inc.

The gases enter the domain via one of the cylinder's extremities, and exit through the opposite one, traversing its interior longitudinally. The cylinder contains no obstacles that may modify or disturb the gases' natural flow though it.

Domain meshing involves the discretization of the fluid domain in which the flow is simulated. It is a discrete representation of the fluid problem. Mesh selection will

significantly impact convergence, the precision and the time involved in the calculations.

The consequences of this flow scenario are positive: it enables the employment of a structural mesh aligned with the principal direction of flow, as well as enabling monitoring of the drag coefficient as a way of validating the results obtained.

The following aspects must be taken into account (Bakker, 2002):

- Cell density and geometry.
- Aspect ratio and asymmetry.
- Mesh configuration in proximity to the cylinder wall.

As the principal component of the gas flow travels in the direction of the cylinder ends, the geometry can be simplified through the concept of *"axial symmetry"*.

Axial symmetry (also known as rotational, radial or circular symmetry) consists of symmetry around an axis, in which all planes taken about this axis possess identical characteristics.

This property, applied to the geometry of the object in this study enables the transition from 3D (cylinder) to 2D (plane) geometry with a corresponding transition of cylindrical coordinates (r, θ, z) to cartesian coordinates (x, y). This transition results in:

- Simplification of the governing equations.
- Reduction in the number of mesh cells
- Greater convergence stability
- Increase in solution precision
- Reduction in number of iterations and simulation time.

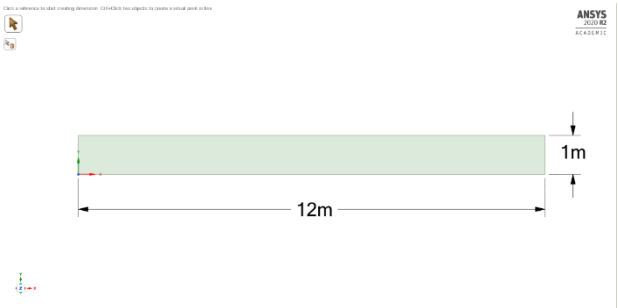

Figure 5. 2D Geometry Exhaust Duct.
Source: Courtesy ANSYS Inc.

Figure 6 and Table 1 below depict mesh characteristics for the fluid problem proposed in this article:

The domain consists of a structured mesh ($3.6 \cdot 10^5$ cells), with a gradual transition from low to high cell density in the direction of the cylinder wall in order to improve flow behaviour predictions in zones in close proximity to the wall.

Table 1: Meshing Quality.
Source: Own Elaboration

Skewness [0 – 1]	Minimum	0.131
	Maximum	0.140
	Average	0.131
	Deviation	0.000
Orthogonality [1 – 0]	Minimum	1.000
	Maximum	1.000
	Average	1.000
	Deviation	0.000
Aspect ratio [1 – …]	Minimum	1.010
	Maximum	16.788
	Average	4.568
	Deviation	4.071
Jacobian relationship [1 – 0]	Minimum	1.000
	Maximum	1.000
	Average	1.000
	Deviation	0.000

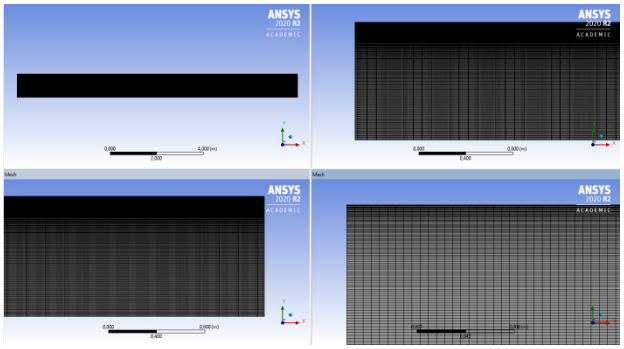

Figure 6. 2D Structural Meshing.
Source: Courtesy ANSYS Inc.

The characteristics contained in Table 1 affect the quality of the mesh in different ways, and it is therefore important to strive for values that best adapt to the given scenario.

To this end, "*skewness*" and "*orthogonality*" parameters near 0 and 1, respectively, are sought. "*Aspect ratio*", where a value of one (1) is considered ideal, is strongly conditioned by the width of cells in proximity to the wall. The parameter *"jacobian relationship"* (geometrical distortion) should also strive for a similarly ideal value of one (1) (Ansys Inc, 2019).

Table 2: Initial Conditions versus Power Level.
Source: Own Elaboration

PL	0	20	40	60	80	100
T7 (K)	515	554	593	633	672	711
c_p (kJ/kgK)	1.09	1.11	1.12	1.13	1.14	1.15
V (m/s)	6.5	9.6	14.2	20.9	30.5	44.5
ρ (kg/m^3)	0.683	0.635	0.593	0.556	0.523	0.495
μ (Pa·s)	2.8E-5	3.0E-5	3.1E-5	3.3E-5	3.4E-5	3.6E-5
ν (m^2/s)	4.1E-5	4.7E-5	5.2E-5	5.9E-5	6.5E-5	7.2E-5
Re	3.2E+5	4.1E+5	5.4E+5	7.1E+5	9.3E+5	1.2E+6

2.5 INITIAL AND BOUNDARY CONDITIONS FOR CONTINOUS PHASE

The solving process is conducted in two stages. The first stage consists of flow modelling on exit from the GT (continuous phase) to determine fluid variable fields (pressure and temperature) in the control volume corresponding to the exhaust. The second stage involves the phase interaction study (continuous – discrete).

Independent of the methodology employed to solve the problem, the continuous phase requires initial and boundary conditions to be specified.

Initial conditions are determined by the fluid variables at time t = 0, or at the first step in the integration scheme. The closer the chosen initial conditions are to the final solution of the problem, the lower the number of iterations that will be required to obtain convergence, thus reducing simulation time and convergence instability.

Table 2, developed from data compiled as described at paragraph 2.2, summarises the initial conditions of the exhaust gases at entry to the fluid domain as a function of GT power level (PL). These can be used to calculate GT exhaust gas pressure and velocity fields.

The following boundary conditions are applicable to the continuous phase (Ansys Inc, 2019):

- Domain entry - *"Velocity – inlet"*.
- Domain exit - *"Pressure – outlet"*.
- Wall - *"Wall"*.
- Axial symmetry axis- *"Axil"*.

These boundary conditions are visually displayed in figure 7 below.

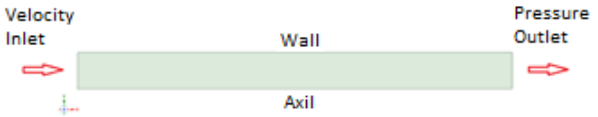

Figure 7. Boundary Conditions Continuous Phase (gas).
Source: Own Elaboration

Boundary conditions *"velocity – inlet"* and *"pressure – outlet"* representing domain entry and exit respectively, are included in the modelling of incompressible flow (low velocity) in which entry velocity and exit pressure are known (in this case atmospheric pressure) (Ansys Inc, 2019).

If velocity is unknown but mass flow at domain entry is known, the *"mass flow inlet"* condition may be used instead. Alternatively by dividing this mass flow value by the duct's cross-sectional area and gas density (incompressible flow only) the *"velocity – inlet"* condition at domain entry can be obtained (Wimshurs, 2018).

It is also possible to employ conditions *"pressure – inlet"* and *"pressure – outlet"* at domain entry and exit as these are known values. The problem with this approach is that the value of the pressure gradient must be exact, so that the velocity field results obtained from application of the conservation of momentum equation satisfy the initial value (Wimshurs, 2018).

2.6 DISCRETE PHASE MODELLING

For the proposed model, Euler-Lagrange (DPM) is selected, where the gaseous phase is considered a continuous medium in which the governing equations are resolved, whilst the discrete phase is resolved by following it through the gaseous (continuous) phase.

The continuous phase is solved in a time-independent, *"steady"* manner, while the discrete phase is solved in a time-dependent, *"transient"* manner, through selection of a given number of continuous phase algorithm iterations for every discrete phase algorithm iteration.

The distribution of spray droplet size is commonly represented by the Rosin-Rammler function, in which the relationship between a given droplet size and the mass fraction of droplets of lesser size is assumed to be exponencial (Lefebvre, McDonell, 2017):

$$1 - Y_D = exp - \left(D/\overline{D}\right)^N \quad (1)$$

where Y_D is the fraction of total volume containing droplets of diameters less than D, D is the selected droplet diameter,

is the distribution's mean droplet diameter (MVD) and N is the droplet diameter's distribution spread parameter:

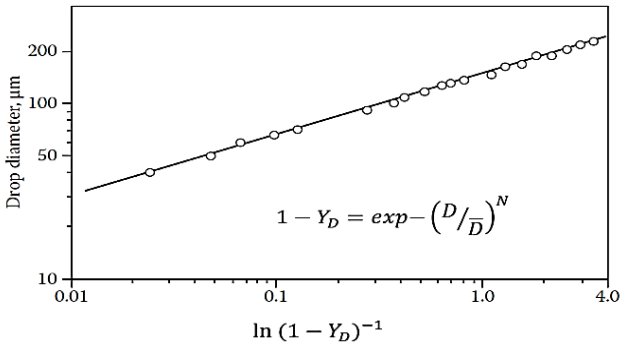

Figure 8. Rosin-Rammler Distribution Representation. Source: Lefebvre, McDonell, 2017

The conversion of cylindrical to cartesian coordinates precludes the use of any given distribution for accurate modelling of the discrete phase. This is a limitation of the selected CFD code, and results in the assumption that the injected particle currents contain droplets of equal size. In essence this assumption is equivalent to the application of a Rosin-Rammler distribution with a high diameter distribution parameter (N).

Modelling of the spray injection pattern is based on the *"hollow cone"* shape as it best approximates the shape of a GT exhaust duct.

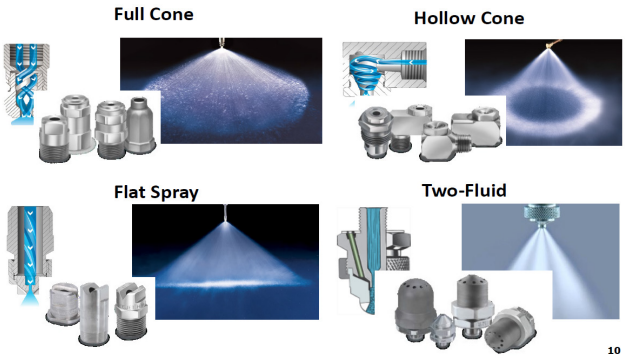

Figure 9. Images of Different Types of Spray Pattern. Source: Schick, 2014

Due to the 2D nature of our model, the hollow cone injection pattern is achieved via a droplet stream injected into the interior of the domain from the axis of symmetry, at a set distance from the entrance, in opposite direction and at a predetermined inclination with respect to the principal direction of exhaust gas flow.

A 2π radian rotation of the previously described 2D geometry about the axis of symmetry will produce a spray pattern of equal-sized droplets and of hollow interior, which mimics the real-world hollow cone pattern described above.

The reason for injection in this manner, specifically against the principal direction of gas flow, is to maximize spray dispersion and phase interaction, maximizing mass, moment and energy transfer within the finite and limited exhaust gas duct.

Table 3: Initial and Boundary Conditions Discrete Phase. Source: Own Elaboration

Initial Conditions Discrete Phase	Fixed	Injection Position (m) Direction Injection Drop Temperature (K) Mass Flow (kg/s)
	Variables	Drop Diameter (µm) Injection speed (m/s) Cone Angle (º)
Boundary Conditions Discrete Phase		Reflect Escape

2.7 INITIAL AND BOUNDARY CONDITIONS FOR DISCRETE PHASE

As per the continuous phase modelling, discrete phase modelling also requires definition of initial and bounday conditions.

In contrast to the continuous phase, discrete phase initial conditions consist of two types: fixed, meaning they remain the same throughout the entire simulation process, and variable, which vary in a sequential manner throughout the simulation process. This variation is introduced in order to determine variable incidence as a function of the observed results, in order to arrive at an optimum parameter combination for the reduction of exhaust gas temperature.

Table 3 below displays a summary of initial and boundary conditions applicable to the discrete phase throughout the calculation process.

The origin of the point of injection, or *"cone vertex"*, must be located on the axis of symmetry, at a set distance (1m in this case) from the the exhaust gas entry into the exhaust domain. This is depicted in Figure 10 below:

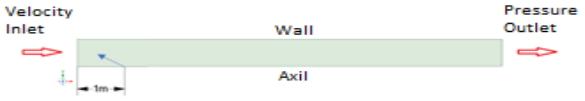

Figure 10. Injection Position and Direction. Source: Own Elaboration

The following boundary conditions are applicable to the discrete phase (Ansys Inc, 2019):

- *"Particle – domain wall"* interaction, "*reflect*" condition.
- *"Particle – domain entry/exit"* interaction, "*escape*" condition.

The reflect condition consists in change in droplet momentum governed by the *"restitution coefficient"* applied to the domain wall (by default $e_n = e_t = 1$). The escape condition allows the discrete phase to exit the domain when domain entry or exit is reached during the discrete phase's trajectory through the domain. Figure 11 below summarises the two types of bounday conditions applicable to the discrete phase (Ansys Inc, 2019).

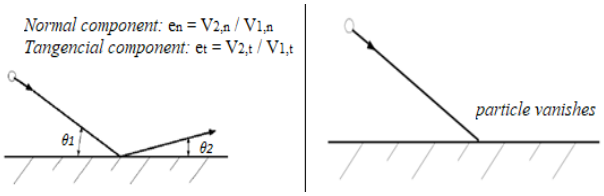

Figure 11. Boundary Conditions Discrete Phase. Source: Ansys Inc, 2019

2.8 SPECIES TRANSPORT

In order to predict the local mass fraction of each species in the discrete phase, Y_i, the following convection-diffusion transport equation must be resolved for each of the individual species (Ansys Inc, 2019):

$$\frac{\partial}{\partial t}(\rho Y_i) + \nabla \cdot (\rho \vec{v} Y_i) = -\nabla \cdot \vec{J}_i + S_i \qquad (2)$$

where is diffusion flow of species *i* and S_i is the growth rate from a dispersed phase.

As the sum of mass fractions of all species in the system must equal unity, the mass fraction of a single species is determined by subtracting the sum of mass fractions of all other species from 1.

When taking into account species transport, the following species (gases) must be considered:

- h2o, in water vapour form.
- o2, as a constituent element of air (21%).
- n2, as a constituent element of air (79%).

Water vapour (h2o) originates in the evaporation and boiling processes during discrete and continuous phase interaction.

Oxygen (o2) and nitrogen (n2) are naturally contained in GT gases as a consequence of the high dilution rates (excess of air) of GT operation.

2.9 VERIFICATION AND VALIDATION

Errors (discretization and linearization) and uncertainties are intrinsic to employment of CFD models, making the development of rigorous methodologies to quantify result confidence levels crucial (Versteeg, Malalasekera, 2007).

In this context, the following AIAA (*"American Institute of Aeronautics and Astronautics"*) terminology definitions are widely accepted (Oberkampf, Trucano, 2002):

- Verification: Consists in evaluating the precision with which a given model represents the developer's conceptual description and model solution.
- Validation: Consists in evaluating the precision with which a given model represents the real world (taking into account the model's intended uses).

Roache defines verification and validation processes with the following phrases (Roache, 1998):

- Verification, *"solving the equations right"*.
- Validation, *"solving the right equations"*.

Verification involves the following steps (Oberkampf, Trucano, 2007):

- *"Sanity checks"*, where the velocity, pressure, etc profiles are confirmed within expected/plausible ranges.
- Confirmation that boundary conditions are satisfied, especially concerning domain entry velocity, exit pressure and velocity in proximity to wall, etc.
- Demonstration that the domain's governing equations satisfy the principles of conservation, namely conservation of mass, moment and energy.
- Linearization error check considered acceptable if governing equation disequilibrium is low.
- Discretization error check, conducted through mesh redefinition and subsequent result confirmation.
- Analytic solution comparison, specifically in zones where flow is considered fully developed with respect to velocity profiles. For pressure values, confirmation of linear decrease along the domain in the direction of flow.

3. RESEARCH OBJECTIVE AND BEHAVIOUR

The aim of this article is to expose the methodology used to study the viability of water mist injection into the interior of marine GT exhaust ducts.

The intent is to reduce exhaust gas temperatures and correspondingly, their contribution to the IR signature of the vessel.

To this end, CFD techniques that predict the behaviour of phase interaction processes in the interior of marine gas turbine exhaust ducts are selected.

The governing equations utilized in the continuous phase calculations for steady, incompressible and isothermic flow in cartesian coordinates and ignoring gravitational effects are described as follows:

$$\nabla \cdot \vec{v} = 0 \tag{3}$$

$$\rho \vec{v} \cdot \nabla \vec{v} = -\nabla p + \mu \nabla^2 \vec{v} \tag{4}$$

For turbulent flow (Re > 2400), characterized by highly fluctuating variable field values, the "Reynolds decomposition" technique must be employed and incorporated into the fluid variable equations as follows:

$$u = \overline{u} + u' \tag{5}$$

$$v = \overline{v} + v' \tag{6}$$

$$p = \overline{p} + p' \tag{7}$$

The final system of equations (in cartesian coordinates) to be solved for the continuous phase, composed of steady, incompressible, isothermic and turbulent flow is:

$$\frac{\partial \overline{u}}{\partial x} + \frac{\partial \overline{v}}{\partial y} = 0 \tag{8}$$

$$\rho\left(\overline{u}\frac{\partial \overline{u}}{\partial x} + v\frac{\partial \overline{u}}{\partial y}\right) = -\frac{\partial p}{\partial x} + \mu\left(\frac{\partial^2 \overline{u}}{\partial x^2} + \frac{\partial^2 \overline{u}}{\partial y^2}\right) + \overline{f}_{turb,x} \tag{9}$$

$$\rho\left(\overline{u}\frac{\partial \overline{v}}{\partial x} + \overline{v}\frac{\partial \overline{v}}{\partial y}\right) = -\frac{\partial p}{\partial y} + \mu\left(\frac{\partial^2 \overline{v}}{\partial x^2} + \frac{\partial^2 \overline{v}}{\partial y^2}\right) + \overline{f}_{turb,y} \tag{10}$$

where $\overline{f}_{turb,x}$ and $\overline{f}_{turb,y}$ represent the force on the flow as a result of turbulence in the x and y directions respectively, estimated from the corresponding RANS *"Reynolds Averaged Navier-Stokes"* model.

Initial and boundary conditions employed in the continuous phase are summarised in Table 4 below.

Table 4: Initial and Boundary Conditions Continuous Phase. Source: Own Elaboration

Steady Flow	$\partial\varphi / \partial t = 0$
Incompressible Flow	ρ = cte.
Isothermic Flow	T = cte.
Turbulent Flow	Re > 2400
Initial Conditions	Table 2
Boundary Conditions	Velocity – inlet
	Pressure – outlet
	Wall
	Axil

Figure 12 below provides a graphical representation of the conditions summarised at Table 4 above.

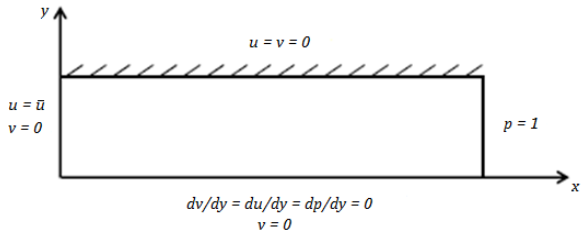

Figure 12. Initial and Boundary Conditions Continuous Phase. Source: Own Elaboration

The phase interaction DPM model must include mass, moment and energy exchanges for both phases, resulting in the following governing equations for the continuous phase:

$$\nabla \cdot \vec{v} = S_m \tag{11}$$

$$\rho \vec{v} \cdot \nabla \vec{v} = -\nabla p + \mu \nabla^2 \vec{v} + \rho \vec{g} + \vec{F}_{DPM} \tag{12}$$

$$\frac{\partial\left(\rho c_p T\right)}{\partial t} + \nabla \cdot \left(\rho \vec{v} c_p T\right) = \nabla \cdot \left(\kappa \nabla T\right) + S_e \tag{13}$$

where terms S_m and S_e (from mass continuity and energy conservation equations) are the source terms corresponding to the phase interaction and $\vec{F}_{DPM}$ corresponds to the force exerted by the discrete phase on the continuous phase as a result of their interaction.

The term S_m is related to the mass lost by the discrete phase and gained by the continuous phase in the form of water vapour, whilst the term S_e is related to the heat lost by the continuous phase and gained by the discrete phase as a result of inert heating, vaporization and boiling processes in the latter phase.

In this case, isothermic flow conditions do not apply, as heat is lost by the continuous phase, resulting in an associated temperature drop within the continuous phase.

Initial and boundary conditions employed in the discrete phase are summarised in Table 5 below:

The viability of the proposal in this article can be explored through experimental quantitative research methods by sequentially varying initial variables of the discrete phase, and numerically comparing them against the results obtained.

Table 5: Fixed - Variables Initial and Boundary Conditions Discrete Phase. Source: Own Elaboration

Fixed Initial Conditions Discrete Phase	Position.- On axis of symmetry one (1) m downstream of inlet
	Direction.- Idem continuous phase and opposite direction
	Discrete phase temperature.- T_0 = 20ºC (293 K)
	Mass flow.- ṁ (variable depending on the power level)
Variables Initial Conditions Discrete Phase	Drop diameter.- Ø = 100, 150 and 200 µm
	Initial velocity.- V = 2x, 3x and 4x relative to velocity inlet
	Semi-angle hollow cone.- θ = 25º, 35º and 45º
Boundary Conditions Discrete Phase	Reflect
	Escape

4. RESULTS AND DISCUSSION

4.1 RESULTS OF THE CONTINUOUS PHASE MODEL

Due to the large number of cells involved in domain discretization, the results are best displayed in graphical form, to produce an efficient and global appreciation of each of the variables involved.

The following figures are an example of the graphical representation of various fluid variables (pressure and velocity) at a GT PL of 60:

As expected, in Figure 13 linear and decreasing pressure variation is observed along the domain until the value corresponding to the pressure outlet boundary condition is met. This is in line with the aforementioned results verification and validation processes.

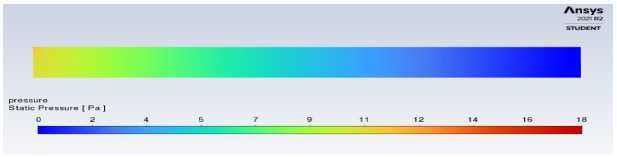

Figure 13. GT Gas Pressure Range in 60 PL.
Source: Courtesy ANSYS Inc.

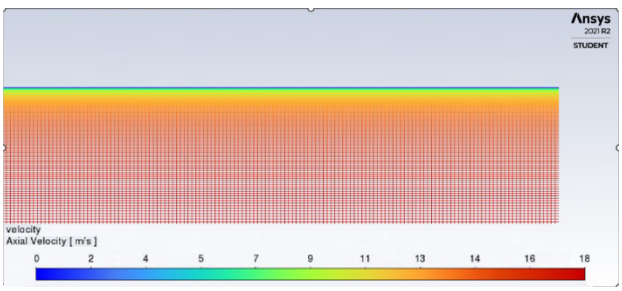

Figure 14. GT Gas Velocity Range in 60 PL.
Source: Courtesy ANSYS Inc.

Figure 14 depicts a large area of the domain which is dominated by axial components of velocity, and governed by convective or inertial effects over diffusive or viscous effects.

In this same figure, the presence of a thin layer adjacent to the cylinder wall and in which velocity is significantly reduced, can be observed. In this zone, inertial and viscous (low Reynolds numbers) effects tend to equalize. This thin layer, the boundary layer, develops on the surface of the wall due to the viscosity of the gases, and in which the gases acquire the same velocity as the wall (no-slip boundary condition).

A great portion of the success of this simulation lies in being able to accurately predict fluid behaviour in regions adjacent to the cylinder wall, characterised by low Reynolds numbers, due to the enormous contribution to friction this region possesses.

4.2 RESULTS OF THE DISCRETE PHASE MODEL

The following figures are an example of phase interaction results for various variables at a GT PL of 60, ṁ = 1.7 kg/s, V = 3x m/s, θ = 35º and Ø = 150 µm.

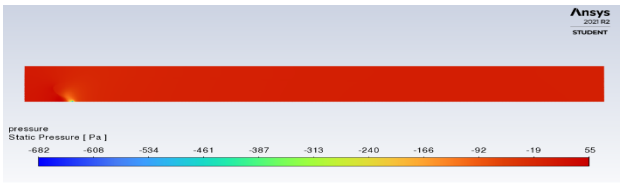

Figure 15. GT Gas Pressure Range in 60 PL
ṁ = 1.7 kg/s, V = 3x m/s, θ = 35º and Ø = 150 µm
Source: Courtesy ANSYS Inc.

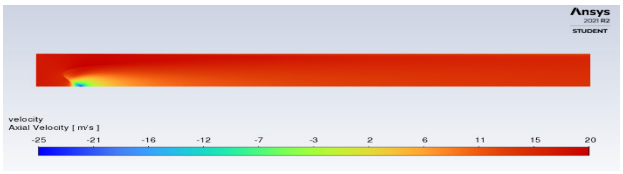

Figure 16. GT Gas Velocity Range in 60 PL
ṁ = 1.7 kg/s, V = 3x m/s, θ = 35º and Ø = 150 µm
Source: Courtesy ANSYS Inc.

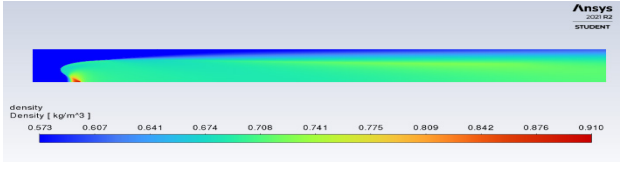

Figure 17. GT Gas Density Range in 60 PL
ṁ = 1.7 kg/s, V = 3x m/s, θ = 35º and Ø = 150 µm
Source: Courtesy ANSYS Inc.

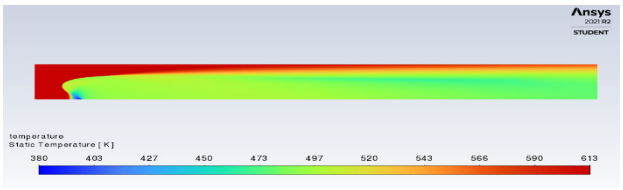

Figure 18. GT Gas Temperature Range in 60 PL
ṁ = 1.7 kg/s, V = 3x m/s, θ = 35º and Ø = 150 µm
Source: Courtesy ANSYS Inc.

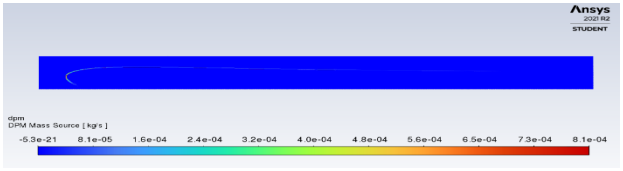

Figure 19. DPM Mass Flow Source in 60 PL,
ṁ = 1.7 kg/s, V = 3x m/s, θ = 35º y Ø = 150 µm
Source: Courtesy ANSYS Inc.

Figures 15 and 16 show how phase interaction processes result in a drop in gas pressure and velocity values (continuous phase) in the region where injection of the discrete phase occurs.

These figures also show how the previously defined boundary condition values for both pressure (pressure outlet = 0 Pa) and velocity (velocity inlet = 20.9 m/s) have remained constant throughout the calculation process (ie. have not been affected by the solver algorithm).

Phase interaction effects on gas density in the continuous phase can be easily observed in Figure 17. In this case, density increases from the discrete phase's point of injection, due to the addition of mass (water) into the less dense continuous phase.

Where temperatures are concerned, Figure 18 shows a reduction at the point of injection of the discrete phase, due to the heat lost by the continuous phase to the discrete phase. The average temperature at domain exit is 523 K, which coincides with an IR suppression level with conventional eductor-difuser based supression systems.

Figure 19 presents discrete phase concentration throughout the domain. It is maximum at the injection zone, steadily reducing until all but disappearing at domain exit.

In this respect, total evaporation of the discrete phase before domain exit is achieved, maximizing the temperature reduction of the continuous phase. This is primarily due to latent heat loss during vaporization (change of state), as opposed to sensible heat loss (change of temperature) from inert heating.

5. CONCLUSIONS

This exposed study allows the following conclusions to be drawn:

- Methodology for the viability study proposed in this article involves two stages: the first consists in modelling of flow in the continuous phase, followed by a second model for the study of phase interaction (continuous – discrete).
- Application of Euler-Lagrange discrete phase model (DPM) establishes the continuous phase as a continuous medium in which the governing equations are solved in a steady state, whilst the discrete phase is solved by considering its passage through the continuous phase as a transient state.
- Concerning the continuous phase, pressure decreases linearly throughout the domain whilst the axial component of velocity is strongly governed by convective or inertial forces, except in zones of close proximity to the wall, in which these forces are balanced by diffusive or viscous effects.
- Concerning the phase interaction study, gas pressure, velocity and temperature value reduction is observed, along with a gas density increase from the point of water mist injection. The change in value of these variables is in line with expectations.
- Average gas temperature at domain exit is compatible confirms the viability of further development of the proposed methodology for its impact on the IR signature of a warship.
- In itself, and in combination with traditional eductor-diffuser-based IR suppression systems, even greater gas temperature reduction targets could be achieved, with associated improvements in the IR susceptibility of a warship.
- The proposed methodology is equally viable in ASMD scenarios, with appropriate dimensioning to suit exhaust gas behaviour at typical warship speeds demanded by these scenarios.

6. REFERENCES

1. ANSYS FLUENT (2019) Theory Guide Release 20.0, ANSYS Inc. Southpointe 2600 ANSYS Drive Canonsburg, PA 15317 Pensilvania, USA.
2. BAKKER, A. (2002) Applied Computational Fluid Dynamics, Lecture 15 - Discrete Phase Model (DPM), ANSYS Inc. Southpointe 2600 ANSYS Drive Canonsburg, PA 15317 Pensilvania, USA.
3. BALLESTEROS, R., GONZÁLEZ, J., et al. (2003) *Técnicas Numéricas en Mecánica*

de Fluidos, Universidad de Oviedo, Rafael Ballesteros Tajadura, Gijón, ISBN 84-607-9546-2.

4. BHASKARAN, R. (2018) *A Hands-on Introduction to Engineering Simulations, Training Documentation*, Swanson Director of Engineering Simulation, Cornell University, Ithaca - New York, USA.
5. CATERPILLAR (2010) *C280 Marine Project Guide*, Peoria, Illinois (USA). https://www.caterpillar.com
6. GE MARINE ENGINES (1999). *Propulsion Gas Turbine System – Technical Manual*, Cincinnati, Ohio (USA).
7. GREIG, A.R., COOMBES, J., et al. (2009). *Modelling the Heat Distribution in a Warship*. Presented al World Maritime Technology Conference (WMTC), Mumbai, India.
8. HISCOKE, B. (2002). *IR Suppression - Exhaust Gas Cooling by Water Injection*. Presented at MECON, Hamburg, Germany, September 2002.
9. LEFEBVRE, A. H. and MCDONELL, V. G., (2017) *Atomization and Sprays*, Second edition, Taylor & Francis CRC Press, ISBN 9781498736251.
10. OBERKAMPF, W. L. and TRUCANO, T. G. (2002) *Verification and Validation in Computational Fluid Dynamics*, Progress in Aerospace Sciences, Vol. 38, ISSN: 0376-0421.
11. OBERKAMPF, W. L. and TRUCANO, T. G. (2007) *Verification and Validation Benchmarks*, Sandia National Laboratories, Albuquerque, California, USA.
12. ROACHE, P. J. (1998) Verification and Validation in Computational Science and Engineering, Hermosa Plublishers, Albuquerque, New México 87119-9110, USA.
13. SCHICK, R., (2014) Simulations in Spray Technology – Innovating in a Rapidly Changing Environnment, Spraying Systems Co., Wheaton, USA.
14. THOMPSON, J., VAITEKUNAS, D., et al. (2000). Lowering Waship Signatures: Electromagnetic and Infrared. Presented at the SMi Conference: Signature Management, February 21 and 22, London.
15. VERSTEEG, H. K. and MALALASEKERA, W. (2007) *An Introduction to Computational Fluid Dynamics - The Finite Volume Method*, 2nd Edition, Pearson Education Limited, USA, ISBN 978-0-13-127498-3.
16. WÄRTSILÄ (2017) *Propulsion Control Systems Specifications*, Wärtsilä Corporation, Helsinki (FIN). https://www.wartsila.com
17. WIMSHURS, A. (2018) *Computational Fluid Dynamics, Fundamentals Course*, Edit. Fluid Mechanics 101.

